Engineering of Magnetic Coupling in Nanographene

Yuqiang Zheng,[1,*] Can Li,[1,*] Yan Zhao,[1] Doreen Beyer,[2] Guanyong Wang,[1] Chengyang Xu,[1] Xinlei Yue,[1] Yupeng Chen,[1] Dan-Dan Guan,[1,3] Yao-Yi Li,[1,3] Hao Zheng,[1,3] Canhua Liu,[1,3] Weidong Luo,[1,4] Xinliang Feng,[2,†] Shiyong Wang,[1,3,‡] and Jinfeng Jia[1,3,§]

[1]*Key Laboratory of Artificial Structures and Quantum Control (Ministry of Education), Shenyang National Laboratory for Materials Science, School of Physics and Astronomy, Shanghai Jiao Tong University, Shanghai 200240, China*

[2]*Center for Advancing Electronics Dresden & Department of Chemistry and Food Chemistry, Technische Universität Dresden, 01062 Dresden, Germany*

[3]*Tsung-Dao Lee Institute, Shanghai Jiao Tong University, Shanghai 200240, China*

[4]*Institute of Natural Sciences, Shanghai Jiao Tong University, Shanghai 200240, China*

(Received 22 September 2019; revised manuscript received 17 January 2020; accepted 13 March 2020; published 10 April 2020)

Nanographenes with sublattice imbalance host a net spin according to Lieb's theorem for bipartite lattices. Here, we report the on-surface synthesis of atomically precise nanographenes and their atomic-scale characterization on a gold substrate by using low-temperature noncontact atomic force microscopy and scanning tunneling spectroscopy. Our results clearly confirm individual nanographenes host a single spin of $S = 1/2$ via the Kondo effect. In covalently linked nanographene dimers, two spins are antiferromagnetically coupled with each other as revealed by inelastic spin-flip excitation spectroscopy. The magnetic exchange interaction in dimers can be well engineered by tuning the local spin density distribution near the connection region, consistent with mean-field Hubbard model calculations. Our work clearly reveals the emergence of magnetism in nanographenes and provides an efficient way to further explore the carbon-based magnetism.

DOI: 10.1103/PhysRevLett.124.147206

Magnetism is mostly associated with the $3d$ or the $4f$ elements, and very rare materials (e.g., Fe, Co, and Ni) are ferromagnets at room temperature. In the past decade, many works reported the emergence of magnetism in carbon-based materials [1–27], and some systems even show Curie temperatures above the room temperature [17,20,24]. Magnetic carbon-based nanostructures are particularly promising for applications in spintronics [1,28], due to the versatility of organic chemical synthesis offering flexible ways to control the structure and tune the magnetic properties, which is hard to achieve from inorganic materials. In addition, carbon-based nanomaterials are expected to have high magnitudes of spin-wave stiffness [29], weak spin-orbit coupling [30], and hyperfine couplings [31] which promise for high temperature magnets, transport of spin-polarized currents [32], and spin-based quantum information processing [1,17,28].

Intuitively, carbon atoms are unlikely to form magnetic order since sp electrons prefer to pair up to form covalent bonds. Theoretical calculations addressing carbon-based magnetism have mainly focused on impurities, point defects, or reduced dimensionality, such as the ferromagnetic order at graphene zigzag edges [32–34], the large net spin in graphene nanostructures with sublattice imbalance [30,34–38], and magnetic order in topological frustrated graphene nanostructures [39,40]. Magnetism of graphene-based materials depends crucially on their atomic structure and surrounding environments. Because of the difficulties encountered in fabricating and characterizing atomically precise graphene nanostructures, the direct comparison between experimental results and theory calculations is impeded, leaving many questions unclear. Thus, it is of great demanding to study the magnetic properties of graphene nanostructures at the atomic level.

In this Letter, we report the engineering of magnetism in atomically precise nanographenes monomers and covalently linked dimers. Scanning tunneling microscopy or spectroscopy (STM/STS), noncontact atomic force microscopy (nc-AFM), together with single particle mean-field Hubbard model and spin-polarized density functional theory (DFT) calculations are combined to determine the magnetic properties of the achieved nanographenes with atomic precision. Our studied nanographenes are fabricated by using the on-surface synthesis approach, which has been widely adopted to prepare atomically precise graphene nanostructures [5,6,11,26,41–44] [see detailed synthesis steps in Supplemental Material [45], Figs. (S1) and (S2)]. Molecular precursors of 9,10-bis(4-bromo-2,6-dimethylphenyl)anthracene were thermally deposited on clean Au(111), and the sample was rapidly annealed to 400 °C to induce C-C addition reactions and cyclodehydrogenation reactions, forming atomically precise magnetic

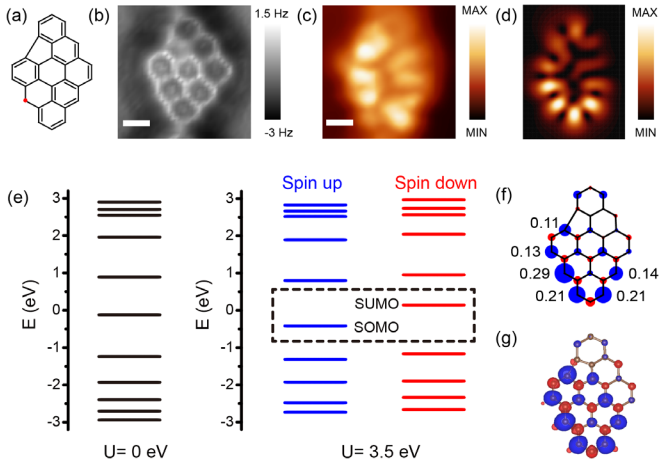

FIG. 1. (a) Chemical structure of achieved nanographene with an embedded five-membered ring. The presence of the five-membered ring breaks the bipartite character of graphene honeycomb lattice. (b) Nc-AFM frequency shift image of an f-NG ($f_0 = 26$ KHz, oscillation amplitude of 80 pm). (c) Constant-height current image (bias voltage: 1 mV). (d) Calculated singly occupied molecular orbital shape. (e) Mean-field Hubbard model calculated energy spectrum. Left:$U = 0$ eV; right:$U = 3.5$ eV. (f) Calculated spin density distribution of f-NG by mean-field Hubbard model. Numbers denote spin density values. (g) Calculated spin density distribution by spin-polarized DFT. The spin delocalizes at the side without the embedded five-membered ring. Blue and red isosurfaces denote spin-up and spin-down density. Scale bars: 0.3 nm.

nanographenes. Afterwards, the sample was transferred to a cryogenic nc-AFM/STM scanner at 4.9 K (1.1K) for characterization.

Figure 1(a) presents the chemical structure of achieved rhombic nanographene with in-total 29 carbon atoms and 13 hydrogen atoms. The pronounced feature of this nanographene is an embedded five-membered ring, which breaks the bipartite character of graphene honeycomb lattice (i.e., two carbon atoms belonging to the same sublattice are directly linked by a single C-C bond). We name the five-membered ring decorated nanographene as f-NG hereafter. Nc-AFM imaging with a CO molecule functionalized tip has been used to resolve the chemical structure of an achieved f-NG [52]. The atomically resolved nc-AFM image in Fig. 1(b) demonstrates that the f-NG is achieved without introducing any unwanted defects. The electronic properties of nanographenes can be well described by the Hubbard Hamiltonian

$$H = -t\sum_{\langle i,j\rangle,\sigma}[c^{+}_{i\sigma}c_{j\sigma} + \text{H.c.}] + U\sum_{i} n_{i\uparrow}n_{i\downarrow},$$

where the operators $c^{+}_{i\sigma}$ and $c_{i\sigma}$ create and annihilate an electron with spin σ at site i with spin $\sigma = \uparrow, \downarrow$, t is the hopping integral between the nearest neighboring sites i and j, and U is the on-site Coulomb repulsion. Here, we performed Hubbard model calculations by using the mean-field approximation [37]. The calculated energy spectra are summarized in Fig. 1(e). Without considering the electron correlation ($U = 0$), the f-NG hosts one singly occupied state. The presence of a single spin in f-NG can also be explained by drawing non-Kekule structures showing one unpaired π electron [cf. Supplemental Material [45], Fig. (S3)]. Including the electron correlation in a mean-field Hubbard model ($U = 3.5$ eV), a Coulomb gap opens, and the spin-up and spin-down energy levels split due to the presence of a net magnetic moment of $S = 1/2$. The computed spin density distribution in Fig. 1(f) reveals that the spin is mostly localized at the zigzag edge carbon atoms of one sublattice rather than the other sublattice. Although the unpaired electron is strongly delocalized, its distribution does not extend over the entire molecule showing pronounced intensity only at the lower side. The computed single occupied molecular orbital (SOMO) shape is presented in Fig. 1(d), which fit very well with the experimental STM image taken at 1 mV bias [cf. Fig. 1(c)]. Spin-polarized DFT calculations have been performed to calculate the electronic structure of f-NG, which reconcile with mean-field Hubbard calculations [cf. Fig. 1(g)].

To confirm the presence of single spins in f-NGs, spatial resolved differential conductance spectroscopy (dI/dV) has been used to probe the spin-related resonances with ultrahigh spatial and energy resolution at low temperature. High-energy dI/dV spectra and STS mapping reveal that f-NGs host singly occupied or unoccupied molecular orbitals, which lie at 0.56 eV below or above the Fermi level, respectively (cf. Supplemental Material [45], Fig. S6). Figure 2(a) presents low-energy dI/dV spectra taken at different positions marked in the inset STM image. All low-energy spectra exhibit a zero-bias peak (ZBP) but with drastically different ZBP intensities. The ZBP intensity can be related to the local density of state (LDOS) intensity of SOMO as shown in the inset, that is, the spin density of f-NG. We attribute this feature to the presence of Kondo resonances due to screening of a localized magnetic moment by Au(111) surface state electrons [7,42,53–56], instead of a LDOS anomaly due to the interaction of states from graphene islands with Rashba Au(111) surface states [57,58]. For comparison, a similar nonmagnetic nanographene has been characterized without observing a zero-bias peak (cf. Supplemental Material [45], Fig. S2). DFT calculations reveal that f-NGs get physiosorbed on Au(111) with an adsorption height of 3.24 Å (cf. Supplemental Material [45], Fig. S5). Since Au(111) hosts Rashba surface states extending quite far into vacuum above Au surface, the observed Kondo resonance in physiosorbed f-NGs should mostly originate from the screening of magnetic impurity by surface state electrons, which can be explained by "Anderson single-impurity model." Under this model, the Kondo resonance is generated very close to the Fermi level with a temperature

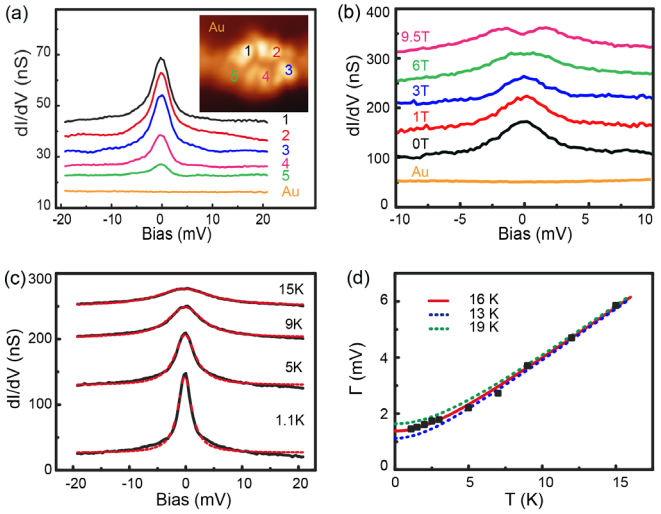

FIG. 2. (a) dI/dV spectra taken at the positions marked by colored numbers in the inset current image (Bias: 1 mV). A Kondo resonance is observed as manifested by a zero-energy peak in dI/dV spectra. The peak intensity is proportional to the spatial spin density intensity. (b) Out-of-plane magnetic field dependence of the Kondo resonance. All dI/dV spectra were taken at the same position. (c) Temperature dependence of the Kondo resonance. All dI/dV spectra were taken at the same position. The dotted lines are simulated curves using a Frota function. (d) The full peak width at half maximum as a function of temperature. A Kondo temperature of 16 K is obtained.

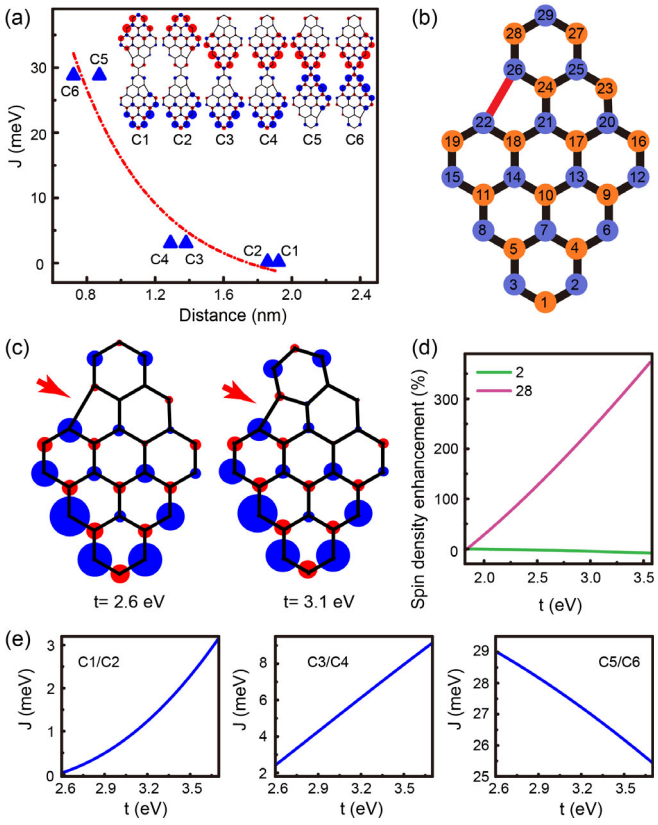

FIG. 3. (a) The magnetic exchange interaction J as a function of the distance between two carbon atoms with the strongest spin density in each unit [the carbon atom No. 8 in (b)]. Inset: spin density distribution of six different f-NG dimers. All dimers exhibit a singlet ground state. Blue and red isosurfaces denote spin up and spin down density. (b) Chemical structure with numbered carbon atoms. The orange and blue solid circles depict sublattice A and B. The red C-C bond breaks the bipartite nature of graphene honeycomb lattice. (c) Left: spin density distributions with the C-C bond length of 1.43 Å; right: with the C-C bond compressed by 5%. (d) Spin density intensity at the carbon atom 2 and 28 as a function of hopping integral t. (e) Magnetic exchange interaction as a function of hopping integral. From left to right: $C1/C2$, $C3/C4$, and $C5/C6$.

dependent peak width. The full width at half maximum (FWHM) can be expressed as $\Gamma = \sqrt{(\alpha k_B T)^2 + (2k_B T_K)^2}$, where T is the temperature, T_K is the Kondo temperature, α is the slope of linear growth of the width at $T \gg T_K$. The obtained temperature dependence of FWHM in Fig. 2(d) can be well fitted by this equation, giving a Kondo temperature of 16 K (with $\alpha = 8.7$) [56]. Further evidences have been obtained by varying the out-of-plane magnetic field. The ZBP splits gradually into two peaks with increased magnetic field, consistent with single-impurity Kondo model.

Engineering of the magnetic coupling is essential to tune the material's magnetic properties. Previous studies found that molecules with a spin $S = 1/2$ did not exhibit any magnetic coupling after self-assembling into molecular dimers or oligomers [42], which, however, may not apply to the covalently coupled molecular oligomers due to π conjugation between molecules. Because of the asymmetric molecular structure, the covalently coupled f-NG dimer has six different configurations (marked as $C1$-$C6$) depending on the positions of two embedded five-membered rings [cf. the inset of Fig. 3(a)]. The electronic states of these six configurations have been calculated using mean-field Hubbard model calculations. When the two five-membered rings face towards each other ($C1$ and $C2$ configurations), the singlet and triplet states are nearly degenerate with the singlet state of a slightly lower energy [cf. Fig. 3(a)]. If the two five-membered rings locate in the same side of each f-NG ($C3$ and $C4$ configurations), the ground state of f-NG dimers is the singlet state with magnetic exchange interaction of 3 meV. Interestingly, the exchange interaction can be further enhanced by putting the two five-membered rings facing against each other ($C5$ and $C6$ configurations), where an exchange energy as large as 29 meV is obtained. This value is larger than the minimal energy dissipation evaluated at room temperature, making the design of room temperature spintronic devices possible [1,28]. The sharp dependence of magnetic exchange interaction on the positions of embedded five-membered rings originates from the inhomogeneous spin density distribution within f-NG monomer. In π conjugated f-NG dimers, the magnetic exchange interaction depends sensitively on the spin

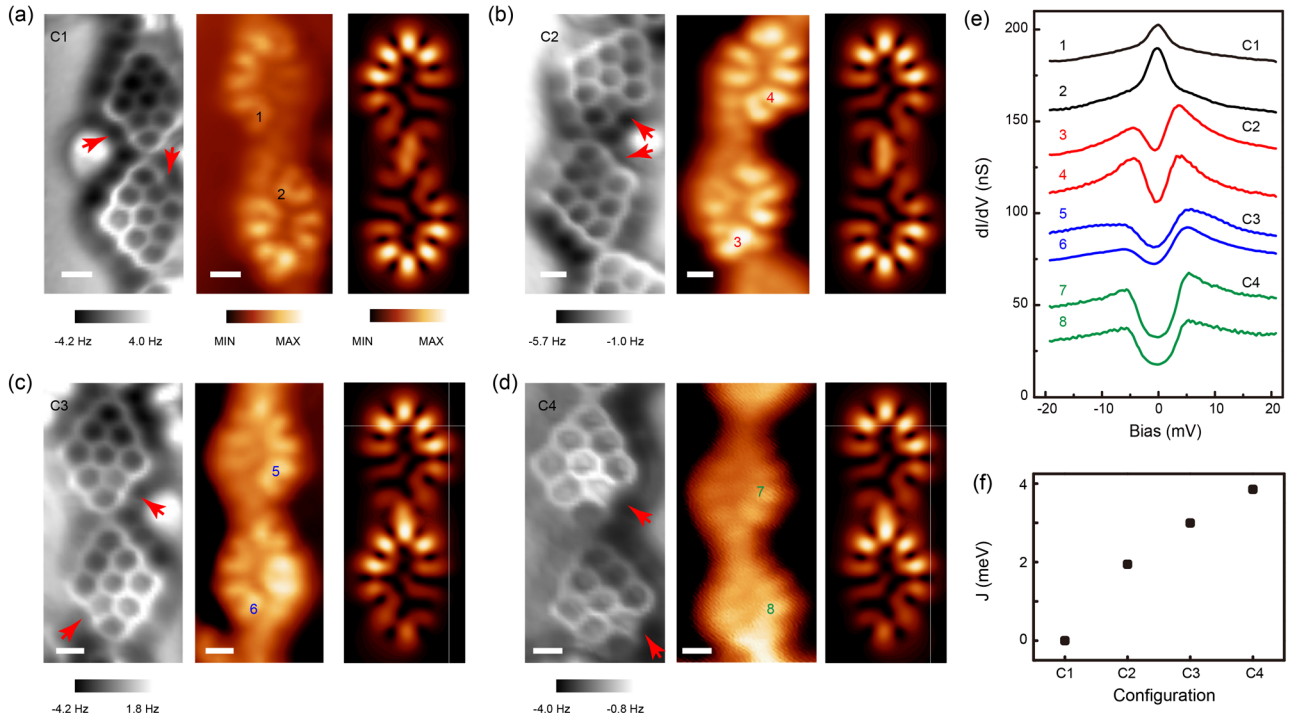

FIG. 4. (a)–(d) Experimental observed four configurations of f-NG dimers named as $C1$-$C4$. Left, nc-AFM frequency shift image ($f_0 = 26$ KHz oscillation amplitude: 80 pm); middle, constant-height current image (bias: 1 mV), and right, simulated STM image. (e) dI/dV spectra taken at the positions marked in (a)–(d). The $C1$ shows a Kondo resonance at both units, suggesting no magnetic coupling at 5 K. The $C2$ shows a magnetic exchange interaction of 2 mV due to the reduced bond length of the C-C bond in embedded five-membered rings, revealing that magnetic exchange energy can be engineered by varying the tilted angle between neighboring units. The $C3$ and $C4$ show a magnetic exchange interaction of 3 and 3.85 meV, confirming that magnetic exchange energy can be engineered by changing the positions of embedded five-membered ring positions. (f) Magnetic exchange energy in $C1$-$C4$. Scale bars: 0.3 nm.

density intensity near the connecting region, that is, wave function overlap of two zero modes [38]. In addition, the magnetic order in f-NG oligomers is also investigated using mean-field Hubbard calculations. As shown in Supplemental Material [45], Fig. S10, an f-NG tetramer and pentamer exhibit a ground state of antiferromagnetic order, allowing for further realization of one-dimensional molecular antiferromagnetic chains with tunable exchange interaction.

The nonbipartite lattice character of f-NG allows for engineering the magnetic exchange interaction by tuning one C-C bond length within the embedded five-membered ring. This bond breaks the bipartite character of graphene honeycomb lattice, and thus changes the spin density distribution at nearby carbon atoms [cf. Figs. 3(b)–3(c)]. To facilitate the following discussion, we number each carbon atom and mark the C-C bond breaking bipartite lattice character in red in Fig. 3(b). Because of the nonbipartite lattice character, the spin density intensity at the carbon atoms No. 23–29 (close to the five-membered ring) enhances dramatically, while the spin density at the carbon atoms No. 1–22 gets slightly quenched as shortening the red C-C bond. Here, we focus on the spin density at the carbon atom No. 2 and No. 28 since these two carbon atoms will affect the magnetic coupling most after forming a dimer. Figure 3(d) reveals that the spin density intensity at the carbon atom No. 28 can achieve a 60% enhancement, while the spin density at the carbon atom No. 2 is reduced by 3% by shortening the C-C bond length by 5%. This unique spin density intensity dependence on the C-C bond length provides an effective way to engineer the magnetic coupling since the exchange interaction of two spins depends sensitively on the spin density overlap at the connecting region (i.e., near the carbon atom No. 2 or No. 28) [38]. For $C1/C2$, a magnetic exchange interaction enhancement of more than 30 times from 0.03 to 0.94 meV is achieved by shortening the bond length by 5% [cf. the left part of Fig. 3(e)]; For $C3/C4$, the magnetic exchange interaction is less sensitive to the C-C bond length [cf. Fig. 3(d)], where a 3 times enhancement is achieved by shortening the bond length of 5% [cf. the middle part of Fig. 3(e)]; For $C5/C6$, the magnetic exchange interaction slightly decreases with the reduced bond length [cf. the right part of Fig. 3(e)]. In addition, the magnetic exchange interaction also depends sensitively on the C-C bond connecting two units, suggesting π conjugation is key to magnetic coupling in f-NG dimers (cf. Supplemental Material [45], Fig. S8). The dependence of magnetic exchange interaction on certain bonds can be understood by considering the spin density overlap near the connecting region in f-NG dimers as changing C-C bond lengths.

Inelastic tunneling spectroscopy has been used to detect the magnetic coupling in f-NG dimers. Inelastic tunneling electrons can excite the ground spin singlet state into a spin triplet state when the energy equals or exceeds the exchange energy between two spins [7,8,19,59]. Usually, dI/dV spectra can reveal such spin-flip inelastic excitation by showing two symmetrical steps at both negative and positive bias voltages, from which one can directly determine the strength of magnetic exchange interaction. As shown in Figs. 4(a)–4(d), four different f-NG dimers have been studied experimentally, denoted as $C1$-$C4$. For the $C1$ configuration, dI/dV spectra in Fig. 4(e) show a pronounced zero-bias Kondo peak on both f-NG units. The observed Kondo resonance suggests that there is no magnetic coupling between two spins at a finite temperature of 5 K, which consists with our calculations giving a negligible magnetic exchange interaction. For the case of the $C2$ configuration, the positions of five-membered rings are similar as that of $C1$, but the two f-NG units are titled with respect to each other forming an angle of 133° between the long axis of two f-NGs. Interestingly, completely different low energy features have been observed on $C2$, where two symmetric steps in dI/dV spectra with onsets at ± 2 meV are clearly resolved. These step features indicate the antiferromagnetic coupling of the two spins with a magnetic exchange interaction of 2 meV (see detailed temperature and magnetic dependence of spin-flip excitation in Supplemental Material [45], Fig. S9) [19,59]. We attribute the emergence of magnetic coupling in $C2$ but not in $C1$ to the tilting of two connecting units. The tilted angle originates from the reduced C-C bond length in the embedded five-membered ring (see detailed C-C bond length analysis in Supplemental Material [45], Fig. S11), in agreement with mean field Hubbard calculations qualitatively [cf. Fig. 3(e)]. For $C3$, dI/dV spectra in Fig. 4(e) reveals that two spins are also antiferromagnetic coupled with each other but with a larger magnetic exchange energy of 3 meV. The obtained larger magnetic exchange interactions than that of $C1$ confirms that the magnetic coupling can be engineered by the positions of embedded five-membered rings [cf. Fig. 3(a)]. For $C4$, the positions of two embedded five-membered rings are similar as that of $C3$, but two f-NG units are more tilted with respect to each other, giving a shorter C-C bond length within the five-membered ring (cf. Supplemental Material [45], Fig. S11). For $C4$, dI/dV spectra in Fig. 4(e) confirm the antiferromagnetic coupling with a slightly larger exchange energy of 3.9 meV than that of $C3$ due to the reduced C-C bond in embedded five-membered rings (cf. Supplemental Material [45], Fig. S11).

In summary, we have demonstrated a successful synthesis and characterization of atomically precise f-NGs. Individual single f-NGs host a single net spin of $S = 1/2$ as confirmed by the Kondo effect. In covalently linked f-NG dimers, two spins are antiferromagnetically coupled with each other, where the magnetic exchange energy can be widely engineered by tuning the local spin density distribution near the connecting region of the dimer. These experimental observations can be nicely reproduced by single electron mean-field Hubbard calculations. Our study provides clear evidences of magnetism in graphene nanostructures, opening new opportunities for further exploration of carbon-based magnetism.

We thank Professor Roman Fasel and Dr. Yalei Lu for fruitful discussions. S. W. acknowledges financial support from the National Natural Science Foundation of China (No. 11874258) and Fok Ying Tung Foundation. This work is also supported by the Ministry of Science and Technology of China (Grants No. 2016YFA0301003 and No. 2016YFA0300403), the National Natural Science Foundation of China (Grants No. 11521404, No. 11634009, No. 11574202, No. 11874256, No. 11790313, No. 11674226, No. U1632102, No. 11674222, No. U1632272, and No. 11861161003), and the Strategic Priority Research Program of Chinese Academy of Sciences (Grant No. XDB28000000).

[*] These authors contributed equally to this work.
[†] Corresponding author.
xinliang.feng@tu-dresden.de
[‡] Corresponding author.
shiyong.wang@sjtu.edu.cn
[§] Corresponding author.
jfjia@sjtu.edu.cn

[1] W. Han, R. K. Kawakami, M. Gmitra, and J. Fabian, Nat. Nanotechnol. **9**, 794 (2014).
[2] T. L. Makarova, Semiconductors **38**, 615 (2004).
[3] P. Esquinazi, D. Spemann, R. Höhne, A. Setzer, K.-H. Han, and T. Butz, Phys. Rev. Lett. **91**, 227201 (2003).
[4] J. M. D. Coey, M. Venkatesan, C. B. Fitzgerald, A. P. Douvalis, and I. S. Sanders, Nature (London) **420**, 156 (2002).
[5] S. Wang, L. Talirz, C. A. Pignedoli, X. Feng, K. Müllen, R. Fasel, and P. Ruffieux, Nat. Commun. **7**, 11507 (2016).
[6] N. Pavliček, A. Mistry, Z. Majzik, N. Moll, G. Meyer, D. J. Fox, and L. Gross, Nat. Nanotechnol. **12**, 308 (2017).
[7] J. Paaske, A. Rosch, P. Wölfle, N. Mason, C. M. Marcus, and J. Nygård, Nat. Phys. **2**, 460 (2006).
[8] J. Li, N. Merino-Díez, E. Carbonell-Sanromà, M. Vilas-Varela, D. G. de Oteyza, D. Peña, M. Corso, and J. I. Pascual, Sci. Adv. **4**, eaaq0582 (2018).
[9] R. R. Nair, I.-L. Tsai, M. Sepioni, O. Lehtinen, J. Keinonen, A. V. Krasheninnikov, A. H. Castro Neto, M. I. Katsnelson, A. K. Geim, and I. V. Grigorieva, Nat. Commun. **4**, 2010 (2013).
[10] M. Sepioni, R. R. Nair, S. Rablen, J. Narayanan, F. Tuna, R. Winpenny, A. K. Geim, and I. V. Grigorieva, Phys. Rev. Lett. **105**, 207205 (2010).
[11] P. Ruffieux, S. Wang, B. Yang, C. Sánchez-Sánchez, J. Liu, T. Dienel, L. Talirz, P. Shinde, C. A. Pignedoli, D. Passerone, T. Dumslaff, X. Feng, K. Müllen, and R. Fasel, Nature (London) **531**, 489 (2016).

[12] C. Tao, L. Jiao, O. V. Yazyev, Y.-C. Chen, J. Feng, X. Zhang, R. B. Capaz, J. M. Tour, A. Zettl, S. G. Louie, H. Dai, and M. F. Crommie, Nat. Phys. **7**, 616 (2011).
[13] Y. Morita, S. Suzuki, K. Sato, and T. Takui, Nat. Chem. **3**, 197 (2011).
[14] K. M. McCreary, A. G. Swartz, W. Han, J. Fabian, and R. K. Kawakami, Phys. Rev. Lett. **109**, 186604 (2012).
[15] R. R. Nair, M. Sepioni, I.-L. Tsai, O. Lehtinen, J. Keinonen, A. V. Krasheninnikov, T. Thomson, A. K. Geim, and I. V. Grigorieva, Nat. Phys. **8**, 199 (2012).
[16] J. J. Palacios, J. Fernández-Rossier, and L. Brey, Phys. Rev. B **77**, 195428 (2008).
[17] K. Bader, D. Dengler, S. Lenz, B. Endeward, S.-D. Jiang, P. Neugebauer, and J. van Slageren, Nat. Commun. **5**, 5304 (2014).
[18] M. Warner, S. Din, I. S. Tupitsyn, G. W. Morley, A. M. Stoneham, J. A. Gardener, Z. Wu, A. J. Fisher, S. Heutz, C. W. M. Kay, and G. Aeppli, Nature (London) **503**, 504 (2013).
[19] J. Li, S. Sanz, M. Corso, D. J. Choi, D. Peña, T. Frederiksen, and J. I. Pascual, Nat. Commun. **10**, 200 (2019).
[20] M. Atzori, L. Tesi, E. Morra, M. Chiesa, L. Sorace, and R. Sessoli, J. Am. Chem. Soc. **138**, 2154 (2016).
[21] M. Coey and S. Sanvito, Phys. World **17**, 33 (2004).
[22] H. Gonzalez-Herrero, J. M. Gomez-Rodriguez, P. Mallet, M. Moaied, J. J. Palacios, C. Salgado, M. M. Ugeda, J.-Y. Veuillen, F. Yndurain, and I. Brihuega, Science **352**, 437 (2016).
[23] G. P. Eyer, K. R. Kittilstved, and T. L. Andrew, J. Phys. Chem. C **121**, 24929 (2017).
[24] J. Červenka, M. I. Katsnelson, and C. F. J. Flipse, Nat. Phys. **5**, 840 (2009).
[25] A. L. Kuzemsky, Int. J. Mod. Phys. B **27**, 1330007 (2013).
[26] S. Mishra, D. Beyer, K. Eimre, J. Liu, R. Berger, O. Gröning, C. A. Pignedoli, K. Müllen, R. Fasel, X. Feng, and P. Ruffieux, J. Am. Chem. Soc. **141**, 10621 (2019).
[27] Z. Sun and J. Wu, J. Mater. Chem. **22**, 4151 (2012).
[28] O. V. Yazyev and M. I. Katsnelson, Phys. Rev. Lett. **100**, 047209 (2008).
[29] D. M. Edwards and M. I. Katsnelson, J. Phys. Condens. Matter **18**, 7209 (2006).
[30] O. V. Yazyev, Rep. Prog. Phys. **73**, 056501 (2010).
[31] B. Trauzettel, D. V. Bulaev, D. Loss, and G. Burkard, Nat. Phys. **3**, 192 (2007).
[32] Y.-W. Son, M. L. Cohen, and S. G. Louie, Nature (London) **444**, 347 (2006).
[33] J. Jung and A. H. MacDonald, Phys. Rev. B **79**, 235433 (2009).
[34] R. Ortiz, J. L. Lado, M. Melle-Franco, and J. Fernández-Rossier, Phys. Rev. B **94**, 094414 (2016).
[35] O. V. Yazyev, in *Basic Physics of Functionalized Graphite*, edited by P. D. Esquinazi (Springer International Publishing, Cham, 2016), pp. 1–24.
[36] O. V. Yazyev, R. B. Capaz, and S. G. Louie, Phys. Rev. B **84**, 115406 (2011).
[37] E. H. Lieb, Phys. Rev. Lett. **62**, 1201 (1989).
[38] R. Ortiz, R. A. Boto, N. García-Martínez, J. C. Sancho-García, M. Melle-Franco, and J. Fernández-Rossier, Nano Lett. **19**, 5991 (2019).
[39] P. Cui, Q. Zhang, H. Zhu, X. Li, W. Wang, Q. Li, C. Zeng, and Z. Zhang, Phys. Rev. Lett. **116**, 026802 (2016).
[40] W. L. Wang, O. V. Yazyev, S. Meng, and E. Kaxiras, Phys. Rev. Lett. **102**, 157201 (2009).
[41] S. Mishra, M. Krzeszewski, C. A. Pignedoli, P. Ruffieux, R. Fasel, and D. T. Gryko, Nat. Commun. **9**, 1714 (2018).
[42] L. L. Patera, S. Sokolov, J. Z. Low, L. M. Campos, L. Venkataraman, and J. Repp, Angew. Chem., Int. Ed. **58**, 11063 (2019).
[43] O. Gröning, S. Wang, X. Yao, C. A. Pignedoli, G. Borin Barin, C. Daniels, A. Cupo, V. Meunier, X. Feng, A. Narita, K. Müllen, P. Ruffieux, and R. Fasel, Nature (London) **560**, 209 (2018).
[44] D. J. Rizzo, G. Veber, T. Cao, C. Bronner, T. Chen, F. Zhao, H. Rodriguez, S. G. Louie, M. F. Crommie, and F. R. Fischer, Nature (London) **560**, 204 (2018).
[45] See Supplemental Material at http://link.aps.org/supplemental/10.1103/PhysRevLett.124.147206 for details of experiments and calculations, which includes Refs. [46–51].
[46] D. Beyer, S. Wang, C. A. Pignedoli, J. Melidonie, B. Yuan, C. Li, J. Wilhelm, P. Ruffieux, R. Berger, K. Müllen, R. Fasel, and X. Feng, J. Am. Chem. Soc. **141**, 2843 (2019).
[47] E. Clar, Chem. Ber. **82**, 46 (1949).
[48] M. Plihal and J. W. Gadzuk, Phys. Rev. B **63**, 085404 (2001).
[49] T. A. Costi, Phys. Rev. Lett. **85**, 1504 (2000).
[50] M. Ternes, New J. Phys. **17**, 063016 (2015).
[51] Q. Fan, D. Martin-Jimenez, S. Werner, D. Ebeling, T. Koehler, T. Vollgraff, J. Sundermeyer, W. Hieringer, A. Schirmeisen, and J. M. Gottfried, J. Am. Chem. Soc. **142**, 894 (2020).
[52] L. Gross, F. Mohn, N. Moll, P. Liljeroth, and G. Meyer, Science **325**, 1110 (2009).
[53] J. Kondo, Prog. Theor. Phys. **32**, 37 (1964).
[54] K. Nagaoka, T. Jamneala, M. Grobis, and M. F. Crommie, Phys. Rev. Lett. **88**, 077205 (2002).
[55] M. Ternes, A. J. Heinrich, and W.-D. Schneider, J. Phys. Condens. Matter **21**, 053001 (2009).
[56] Y. Zhang, S. Kahle, T. Herden, C. Stroh, M. Mayor, U. Schlickum, M. Ternes, P. Wahl, and K. Kern, Nat. Commun. **4**, 2110 (2013).
[57] Y. Li, D. Subramaniam, N. Atodiresei, P. Lazić, V. Caciuc, C. Pauly, A. Georgi, C. Busse, M. Liebmann, S. Blügel, M. Pratzer, M. Morgenstern, and R. Mazzarello, Adv. Mater. **25**, 1967 (2013).
[58] P. Leicht, J. Tesch, S. Bouvron, F. Blumenschein, P. Erler, L. Gragnaniello, and M. Fonin, Phys. Rev. B **90**, 241406 (2014).
[59] G. Czap, P. J. Wagner, F. Xue, L. Gu, J. Li, J. Yao, R. Wu, and W. Ho, Science **364**, 670 (2019).